26th International Congress on Modelling and Simulation, Adelaide, SA, Australia, 30 Nov–4 Dec 2025
mssanz.org.au/modsim2025

Including flooded vegetation in Earth-observation flood maps to assist in the assessment of hydrological models

CJ Ticehurst [a], **Jai Vaze** [a], **Mahdi Montazeri** [b], **Cherry Mateo** [a], **Chi Nguyen** [a]

[a] *CSIRO Environment, Canberra, Australian Capital Territory,* [b] *CSIRO Environment, Adelaide, South Australia*
Email: Catherine.Ticehurst@csiro.au

Abstract: Hydrodynamic models can provide accurate and detailed information about spatial extents of flood events. Their success depends on reliable calibration and validation data to fine-tune the model and assess the results. Earth observation data are often included in this process. Optical data such as Landsat, MODIS and more recently Sentinel-2 imagery are often used for this purpose and have proven their success at mapping the extent of open water. Identifying flooded vegetation is possible, but more complex. Another challenge is that flood events are often associated with cloud cover, which can greatly reduce the quantity and quality of flood maps that can be derived from these sensors. Synthetic Aperture Radar (SAR) instruments are not affected by cloud cover, and their backscatter signal is influenced by the land and water that they interact with. The Sentinel-1 SAR sensor is often used to map flood extent, which it does successfully for large, open and smooth water bodies. This study investigates the capability of the Landsat, Sentinel-2 and Sentinel-1 sensors at identifying flooded vegetation, which is then combined with open water flood extent. The agreement of these flood maps with the extents produced from a hydrodynamic model are assessed, along with the more traditional open water flood maps. The results show a better agreement between the Landsat/Sentinel-2 flood extents and the hydrodynamic model when flooded vegetation is included. There is a small improvement in agreement between the Sentinel-1 water maps and the hydrodynamic model when flooded vegetation is included, however the commission errors can increase substantially.

Keywords: *Inundation extent, remote sensing, Synthetic Aperture Radar*

1. INTRODUCTION

Flood events are becoming more frequent and more extreme around the world (Berghuijs et al., 2017), requiring increased attention to methods for flood mitigation and monitoring (Lerat and Vaze, 2025). While hydrodynamic (HD) models may be slow to run and require large computing resources, they can produce accurate results at a high spatial resolution and frequent temporal scale (Teng et al., 2017). Achieving these good results requires quality calibration and validation information about flood water height and extent, through the use of stream flow observations and water extent derived from Earth observation data. Earth observation data can provide quality information about water extent over large areas at discrete points in time (Pekel et al. 2016), however the more commonly used optical remote sensing data (e.g. Landsat, MODIS and Sentinel-2) are affected by cloud cover. This greatly reduces the volume of quality images that can help in the assessment of HD models.

Despite the influence of cloud cover on optical remote sensing imagery, cloud-free data has been successfully acquired and used to map flood events around the world (Brakenridge and Anderson 2006). One of the more common methods of identifying surface water in optical imagery is to use water indices, such as the modified Normalised Difference Water Index (mNDWI; Xu, 2006) or a multi-band water index developed by Fisher et al. (2016) (called WI_{2015}). These are successful at identifying open water, but not flooded vegetation, which can impact its usefulness in the calibration and validation of hydrological models built around flooded forests and wetlands. To help overcome this, Dunn et al. (2023) developed a threshold based on the Tasselled Cap Wetness Index (TCW) that has been calibrated using a selection of wetlands. Lymburner et al. (2024) uses the relationship between the Landsat and Sentinel-2 Shortwave Infrared bands and persistent canopy cover for successfully identifying flooded wooded wetlands.

Synthetic Aperture Radar (SAR) sensors use microwave wavelengths, hence are not affected by cloud cover. The SAR backscatter is relatively low over large, calm open water, enabling the identification of surface water (Bioresita et al. 2018). The co-polarised bands (i.e. HH = horizontally transmitted and received signal, and VV = vertically transmitted and received) are generally found to provide a better estimate of inundation extent, with HH considered to be the best of the two (Grimaldi et al., 2020). However, in certain cases the cross-polarised band performs better (Ticehurst et al., 2023). The Sentinel-1 SAR has been operational since 2016, acquiring data every 6–12 days (although this frequency reduced when Sentinel-1B ceased to operate in 2022) at a near-global scale. It has been shown to be able to identify large flood events (Twele et al, 2016). However, its C-band wavelength (~5.6cm) means it has difficulty identifying shallow flood water due to its rough surface (Ticehurst and Karim, 2023), and the SAR signal can be attenuated in dense overhead vegetation.

Severe floods have affected the Richmond catchment in the Northern Rivers region in northern NSW (Australia) in recent years, including an unprecedented event in February/March 2022, which severely impacted the city of Lismore. This provided the catalyst for developing a hydrodynamic model for the Richmond catchment, and the collection of all available Earth observation data to assist in this process. HD models have been often assessed using open water extent derived from Earth observation data (Karim et al. 2024). However, in heavily vegetated areas, the water extent derived from Earth observation data without accounting for flooded vegetation can limit its usefulness in assessing HD models. This study investigates the agreement between the HD model water extents and those derived from Earth observation sensors, when deriving open water alone and open water plus flooded vegetation. It investigates water extent derived from optical remote sensing data (Landsat and Sentinel-2) as well as Sentinel-1 SAR.

2. DATA AND METHODS

2.1. Study area

The Richmond catchment in the Northern Rivers region is located in the northeast of NSW (Australia) (Figure 1). The study area is centred around the township of Coraki in the lower section of the catchment and covers 150,000 ha. This is the location where the Wilson River, which runs through the city of Lismore, meets the Richmond River downstream from Casino. The Bungawalbyn Creek joins the Richmond River a further 8 km downstream from this junction. The study area consists mostly of agricultural areas used for farming livestock and growing crops. Approximately 30% of the study area is forested including national parks and state forests as well as important wetlands.

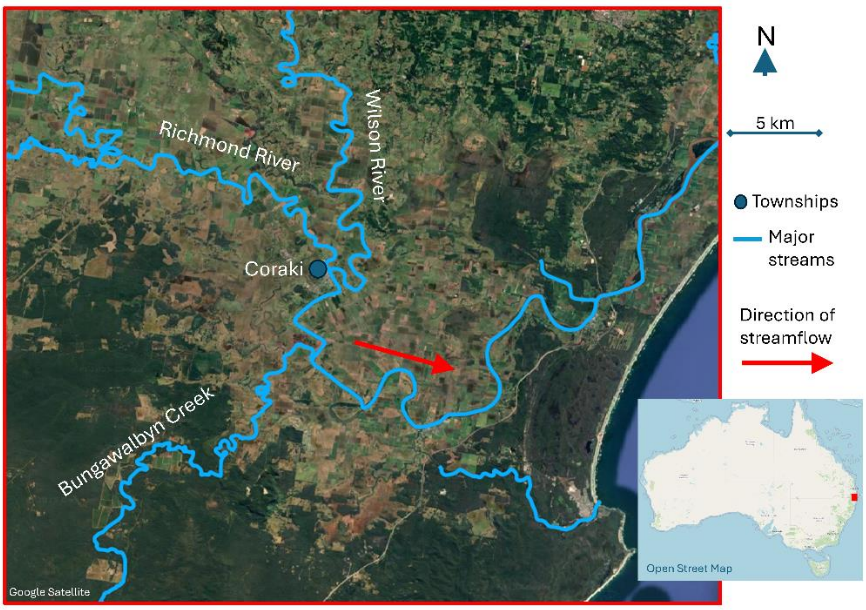

Figure 1 Study site shown on Google Satellite background, including major streams. The inset shows the location of the study site in red box

2.2. Hydrodynamic model

The 2-dimensional MIKE 21FM hydrodynamic model was used to model flood extent in the Richmond catchment. Rather than using observed streamflow at multiple point locations, the model uses hourly spatial rainfall to generate spatial runoff across the catchment (Vaze et al., 2025). The model was used to generate water velocity and water depth for five flood events: December 2007–January 2008 (with a 1 in 8 year return period); May–June 2009 (with a 1 in 12 year return period); January–February 2013 (with a 1 in 4 year return period); March–April 2017 (with a 1 in 21 year return period); and February–April 2022 (which was maximum on record). Water velocity and water depth was estimated for every 10 m x 10 m grid cell at 3-hourly intervals. A comparison of the modelled and observed water levels at the streamflow gauge at the centre of the study site (flow gauge number 203403 at Coraki) has an R^2 and Nash-Sutcliffe Efficiency (NSE) of 0.988 and 0.960 for the 2017 flood event, and an R^2 and NSE of 0.983 and 0.923 for the 2022 flood event (Vaze et al., 2025).

The modelled flood events for 2017 (26 March to 15 April) and 2022 (20 February to 15 April) are compared to the Earth observation data in this study. Modelled water extent is defined as water depth greater than 0.05 m.

2.3. Landsat and Sentinel-2 data

Landsat and Sentinel-2 data are available through Digital Earth Australia (DEA; https://www.ga.gov.au/scientific-topics/dea/dea-data-and-products) in an analysis ready format, meaning they are spatially consistent through time and have been atmospherically corrected as well as normalised for sun angle effects. Landsat 8 and 9 Operational Land Imagers are currently operating at full capacity, and each provide data every 16 days at a spatial resolution of 30 m, while Sentinel-2 (from sensors A and B) provide data every five days at a spatial resolution of 10–20 m, depending on the wavelength. All available Landsat and Sentinel-2 data were inspected for the 2017 and 2022 flood events, however cloud cover greatly reduced the number of quality images.

The mNDWI (Xu, 2006) was used to create maps of open water extent (referred to as 'open water' (OW)), with values above zero defined as water. The Tasseled Cap Wetness Index (TCW) was used to identify flooded vegetation using the method of Dunn et al. (2019). The TCW is good at identifying flooded vegetation, however it can also misclassify cloud shadow, terrain shadow and heavily vegetated areas as flooded. To reduce this error, additional masking was applied to the Landsat and Sentinel-2 water maps to remove areas unlikely to flood (i.e. uplands and steep terrain as identified in a Digital Elevation Model (DEM)) as well as areas where vegetation was too dense to detect flood water (identified where the Normalised Difference Vegetation Index was >0.8). A variable Shortwave Infrared (SWIR-2) threshold was used to mask pixels likely to be vegetation canopy shadow (using the values of Lymburner et al., 2024). The areas of flooded vegetation were added to the open water flood maps (referred to as 'open plus flooded vegetation' (O+FV)). Clouds and cloud shadow were masked from the images using the standard fmask band accompanying each image. In some cases, clouds and cloud shadow was not always captured in the cloud/cloud shadow mask, so these were manually excluded.

2.4. Synthetic Aperture Radar data

Sentinel-1 backscatter data are available through the European Space Agency data hub (https://dataspace.copernicus.eu/). The Sentinel-1 data are captured over the same area every 12 days using its standard acquisition mode. These were processed to an analysis-ready format (radiometrically corrected and orthorectified) of normalised radar backscatter (Gamma nought), as well as filtered to reduce speckle effects. The Sentinel-1 data have a pixel size of 10 m x 10 m and are dual polarised with a VV and VH band (V=vertical and H=horizontal).

To identify open water in the Sentinel-1 images the cross polarised band was used (i.e. VH). A low backscatter threshold (automatically derived within each image using the OTSU algorithm (Otsu, 1979) over a permanent water body) was used to extract open surface water, and small 'clumps' of pixels (i.e. less than 100 pixels) removed as these are often misclassified as water bodies. A DEM was used to mask the upland areas and the Height Above Nearest Drainage method (HAND; Nobre et al., 2011) was used to exclude steep terrain since these areas are unlikely to flood. These flood maps are referred to as 'open water' (OW).

Flooded vegetation often has a strong double bounce response in SAR imagery, leading to an increase in backscatter for the co-polarised bands (i.e. VV for Sentinel-1). This increase was found to be minimal in the Sentinel-1 imagery for the study site, so a non-flooded image was used to help detect areas where there was an increase in backscatter from the dry to flooded images. A trial-and-error process was used to select a threshold to identify flooded vegetation. Like in the open water image, small clumps of pixels (less than 100 pixels) were removed, and the DEM and HAND were used to mask upland areas and steep terrain respectively. The remaining areas were added to the open water images to create the 'open plus flooded vegetation' (O+FV) flood maps.

2.5. Hydrodynamic model and Earth observation comparisons

Table 1 shows all the water maps derived from Earth observation data that were compared with the HD model. The Earth observation data selected for comparison with the HD model were (mostly) free of cloud and had (near) full coverage of the study site. The Earth observation results used in these comparisons were for both the 'open water' (OW) flood maps and the 'open plus flooded vegetation' (O+FV) flood maps. Each row shows the date and time of the HD model, and the Earth observation image it was compared to. The green cells show an additional comparison between the Sentinel-2 and Sentinel-1 data (which only had partial coverage of the study site) acquired on the same date (but different time).

The HD model water extent was compared to the 'open water' (OW) and 'open plus flooded vegetation' (O+FV) for all the non-coloured rows in Table 1. The producer's accuracy, user's accuracy and F1 score (Maxwell and Warner, 2020) was used to assess agreement between the two flood maps. For this study, the producer's accuracy, ranging from zero to one, is an indication of omission errors. (i.e. values near zero mean the Earth observation flood maps missed a lot of water compared to the HD model). The user's accuracy indicates commission errors (i.e. values near zero mean the Earth observation flood maps identified a lot more water compared to the HD model). The F1 score is a function of the producer's and user's accuracies with values ranging from near zero (poor agreement) to one (perfect agreement). One water map from each sensor, acquired during extensive flooding, was also overlaid onto the HD model for a spatial comparison.

Table 1 Date and hour (in brackets) of acquisition of Earth observation images and Hydrodynamic (HD) model water extents used in comparison analysis. The green row shows the two Earth observations that were compared

HD model	Landsat	Sentinel-2	Sentinel-1
2017-04-07 (09)	2017-04-07 (10)		
2022-03-03 (06)			2022-03-03 (05)
2022-04-01 (12)		2022-04-01 (11)	
2022-04-05 (09)	2022-04-05 (10)		
2022-04-08 (06)			2022-04-08 (05)
2022-04-11 (09)		2022-04-11 (10)	
		2022-04-01 (11)	2022-04-01 (05)

3. RESULTS

3.1. Open water and open-plus-flooded-vegetation comparisons with the Hydrodynamic model

Table 2 shows the F1 scores along with the producer's and user's accuracies for the six Earth observation flood maps compared to the HD model for open water (OW) and open plus flooded vegetation (O+FV). A spatial comparison of the HD model with Landsat (Figure 2a and b), Sentinel-2 (Figure 2c and d) and Sentinel-1 (Figure 2e and f) show where these main differences occur. The results show a large improvement in agreement when O+FV is used instead of just OW for the Landsat and Sentinel-2 flood maps. There is a much smaller improvement in agreement when O+FV is used instead of OW for Sentinel-1.

While the F1 score increases between the OW and O+FW comparisons, the user's accuracy reduces for all six examples. This is indicating that the Earth observation data are identifying water in areas where the HD model isn't. For the Landsat and Sentinel-2 data, this difference occurs around the edges of wetlands or in agricultural areas where soils may be saturated with water that are not necessarily flooded. For Sentinel-1 this difference is scattered across the floodplain and may be more related to the type and amount of vegetation cover rather than flood water. Even with the inclusion of flooded vegetation, Sentinel-1 is still more likely to underestimate water extent compared to the HD model.

3.2. Comparison of Earth observation water extents

One Sentinel-2 image was acquired on the same date as a Sentinel-1 image (2022-04-01), separated by six hours. A spatial comparison of the open water extents (OW) shows very similar results (Figure 3a) with a high F1 score of 0.85. The producer's accuracy and user's accuracy is 0.76 and 0.98 respectively, with the Sentinel-2 identifying a little more water compared to Sentinel-1. The agreement between the two reduces when flooded vegetation (O+FV) is included in the water extent with an F1 score of 0.74. The producer's and user's accuracy decrease to 0.59 and 0.96 respectively, mainly because Sentinel-1 is not identifying as much flooded vegetation as Sentinel-2. This further demonstrates the challenge of identifying flooded vegetation in Sentinel-1 SAR.

Table 2 F1 score (with producer's accuracy / user's accuracy in brackets) for comparison of Hydrodynamic model and Earth observation water extents for open water (OW) and open water plus flooded vegetation (O+FV)

Date	Sensor	OW	O+FV
2017-04-07	Landsat	0.55 (0.40/0.87)	0.69 (0.64/0.74)
2022-04-05	Landsat	0.67 (0.56/0.84)	0.77 (0.77/0.78)
2022-04-01	Sentinel-2	0.76 (0.67/0.88)	0.85 (0.88/0.83)
2022-04-11	Sentinel-2	0.47 (0.32/0.87)	0.64 (0.56/0.75)
2022-03-03	Sentinel-1	0.73 (0.56/0.99)	0.76 (0.62/0.97)
2022-04-08	Sentinel-1	0.45 (0.30/0.94)	0.54 (0.48/0.61)

4. DISCUSSION AND CONCLUSION

Flood maps derived from Earth observation sensors are often used as an independent data source for assessing HD models. Agreement between the two gives greater confidence in the overall results. Inclusion of flooded vegetation in flood maps derived from Landsat and Sentinel-2 data showed an improved agreement when compared to the HD model results for the same dates (and similar times). There was less improvement when flooded vegetation was included in the Sentinel-1 flood maps when compared to the HD model. This was also found when Sentinel-1 O+FV was compared to Sentinel-2, however there was good agreement for open water between Sentinel-1 and Sentinel-2 for the common date.

Using TCW with the method adopted by Dunn et al. (2023) is an effective way of identifying flooded vegetation, however caution needs to be applied when using it due to the potential of high commission errors. Any dark pixels such as residual cloud shadow, steep terrain, and vegetation canopy shadow can be misclassified as water. This is why the method adopted in this study applied a multi-layered mask so that only the areas likely to flood were considered in the TCW algorithm.

The antecedent conditions as well as stage of a flood event will influence the accuracy of the Earth observation data for identifying flood waters, especially in the Sentinel-1 SAR data where areas of high soil moisture can affect the backscatter. In vegetated areas this can result in an increase in backscatter which may resemble flooded vegetation. There are other, more sophisticated approaches to identifying flooded vegetation in SAR data which are worth exploring for this study site. The NovaSAR-1 is an experimental S-band SAR that launched in 2019. The CSIRO has a 10% share in this satellite and can task imagery over the Australian continent, with a particular focus on hazardous events (Zhou et al., 2020). The NovaSAR-1 sensor has a longer wavelength than Sentinel-1 (~9cm), with different imaging modes and tasking priorities, making it potentially valuable for identifying flood events during cloudy periods. Preliminary work has shown that NovaSAR-1 can successfully identify flooded vegetation using its HH polarised band. Further research is required to determine if this is due to the longer wavelength, the steeper viewing angle (reducing the amount of vegetation to penetrate before reaching the ground), or the polarisation of the NovaSAR-1 sensor compared to Sentinel-1 (which has a standard acquisition mode that acquires VV and VH polarisation).

Overall, this study has shown that consideration of flooded vegetation when mapping water extent in Earth observation data is important, especially in wetlands and vegetated floodplains. This gives greater confidence in the use of Earth observation data for the assessment of HD models.

ACKNOWLEDGMENTS

The hydrodynamic model outputs used in the study are from the modelling undertaken as part of the Northern Rivers Resilience Initiative (NRRI) project funded by the National Emergency Management Agency (NEMA).

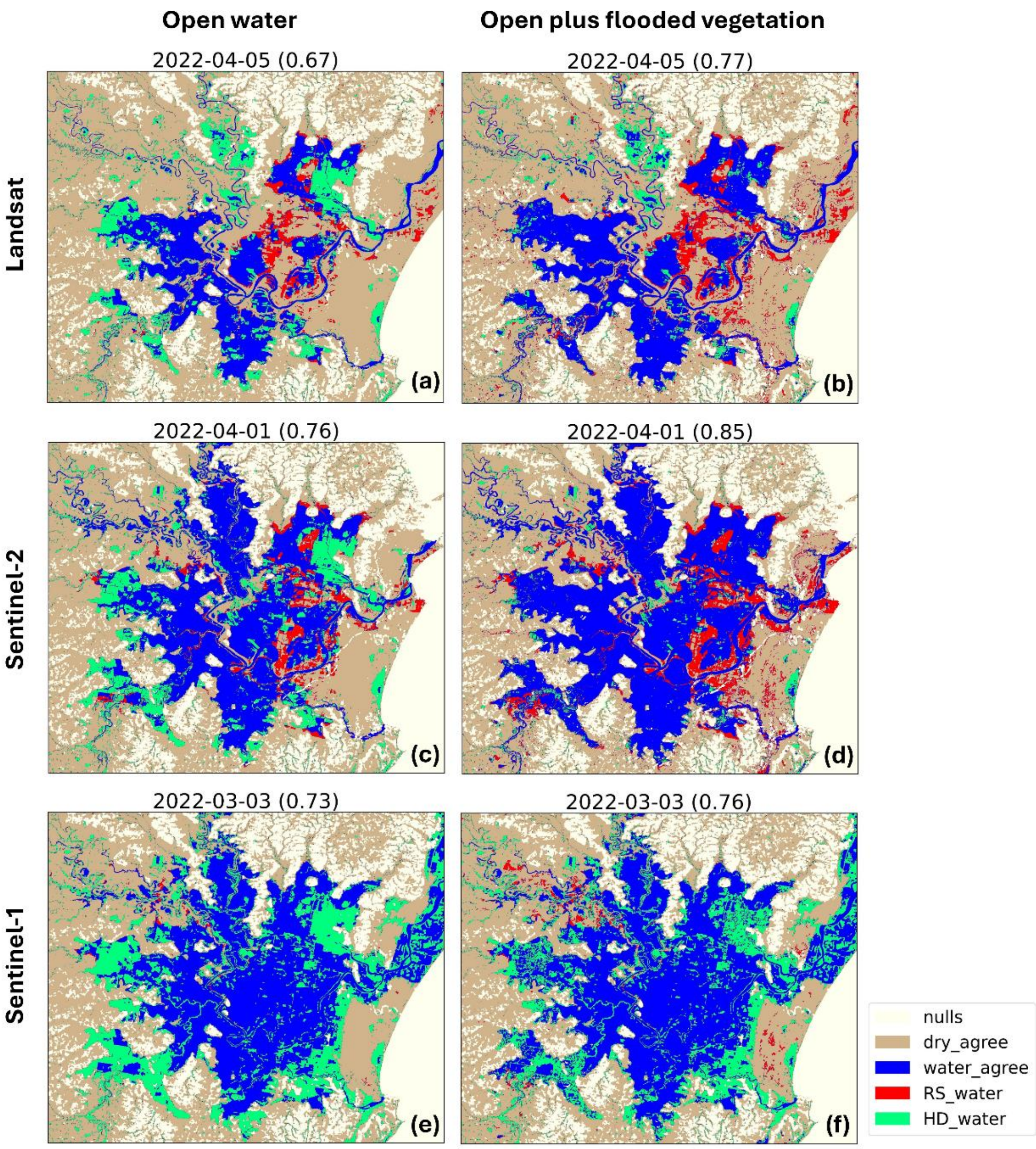

Figure 2 Comparison of Earth observation (RS_water) and Hydrodynamic (HD_water) model water extents from Landsat, Sentinel-2 and Sentinel-1. The left-hand column shows Earth observation water extents for open water only. The right-hand column shows Earth observation water extents for open water plus flooded vegetation. Image date is shown above each image with F1 score in brackets

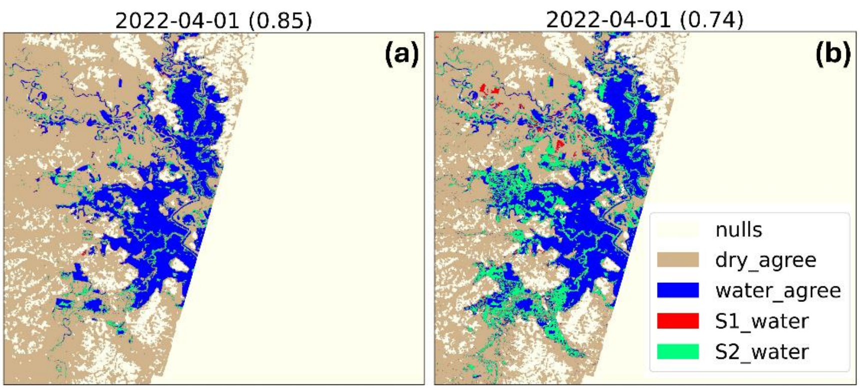

Figure 3 Comparison of Sentinel-1 (S1_water) and Sentinel-2 (S2_water) water extents for (a) open water and (b) open plus flooded vegetation. Image date is shown above each image with F1 score in brackets

REFERENCES

Berghuijs WR, Aalbers EE, Larsen JR, Trancoso R and Woods RA (2017) Recent changes in extreme floods across multiple continents. *Environmental Research Letters.* 12 114035. DOI:10.1088/1748-9326/aa8847.

Bioresita F, Puissant A, Stumpf A and Malet JP (2018) A Method for Automatic and Rapid Mapping of Water Surfaces from Sentinel-1 Imagery. Remote Sensing, 10(2). doi:10.3390/rs10020217.

Brakenridge R and Anderson E (2006) MODIS-based flood detection, mapping and measurement: the potential for operational hydrological applications. Transboundary Floods Reduce Risks Through Flood Management. 72:1–12.

Dunn B. Ai E, Alger MJ, Fanson B, Fickas KC, Krause CE, Lymburner L, Nanson R, Papas P, Ronan M and Thomas RF (2023) Wetlands Insight Tool: Characterising the Surface Water and Vegetation Cover Dynamics of Individual Wetlands Using Multidecadal Landsat Satellite Data. Wetlands 43, 37 (2023). https://doi.org/10.1007/s13157-023-01682-7.

Fisher A, Flood N, and Danaher T (2016) Comparing Landsat water index methods for automated water classification in eastern Australia. Remote Sensing of Environment, 175: 167–182, doi:10.1016/j.rse.2015.12.055.

Grimaldi S, Xu J, Li Y, Pauwels VRN, Walker JP (2020) Flood mapping under vegetation using single SAR acquisitions, Remote Sensing of Environment, 237, doi:10.1016/j.rse.2019.111582.

Karim F, Kim S, Ticehurst C, Hughes J, Marvanek S, Gibbs M, Yang A, Wang B and Petheram C (2024) Floodplain inundation mapping and modelling for the Victoria catchment. A technical report from the CSIRO Victoria River Water Resource Assessment for the National Water Grid. CSIRO, Australia.

Lerat J, Vaze J (2025) How February 2022 redefines extreme floods in Australia. Communications Earth and Environment, **6**, 378. https://doi.org/10.1038/s43247-025-02307-z.

Lymburner L, Ticehurst C, Adame MF, Sengupta A and Kavehei E (2024) Seeing the floods through the trees: Using adaptive shortwave infrared thresholds to map inundation under wooded wetlands. Hydrological Processes, 38(6), e15174. https://doi.org/10.1002/hyp.15174.

Maxwell AE and Warner TA (2020) Thematic Classification Accuracy Assessment with Inherently Uncertain Boundaries: An Argument for Center-Weighted Accuracy Assessment Metrics. Remote Sensing, 12, doi:10.3390/rs12121905.

Nobre AD, Cuartas LA, Hodnett M, Renno CD, Rodriguez G, Silveira A, Waterloo M and Saleska S (2011) Height Above the Nearest Drainage – a hydrologically relevant new terrain model, Journal of Hydrology, 2011, 404(1-2), pp. 13–39.

Otsu N (1979) A threshold selection method from gray-level histograms. IEEE Transactions on Systems, Man and Cybernetics, 9(1), 62–66.

Pekel JF, Cottam A, Gorelick N, Belward AS (2016) High-resolution mapping of global surface water and its long-term changes. Nature 540, 418–422. https://doi.org/10.1038/nature20584.

Teng J, Jakeman AK, Vaze J, Croke BFW, Dutta D, Kim S (2017) Flood inundation modelling: A review of methods, recent advances and uncertainty analysis, Environmental Modelling & Software, 90, 201-216, https://doi.org/10.1016/j.envsoft.2017.01.006.

Ticehurst C and Karim F (2023) Towards developing comparable optical and SAR remote sensing inundation mapping with hydrodynamic modelling, International Journal of Remote Sensing, 44:9, 2912-2935, DOI: 10.1080/01431161.2023.2211714.

Ticehurst C, Zheng-Shu Z-S and Parker A (2023). Mapping flood events across Australia using NovaSAR-1 and Sentinel-1. In proceedings of the 2023 IEEE International Radar Conference (RADAR 2023). Sydney, Australia, 6–10 November 2023.

Twele A, Cao W, Plank S, and Martinis S (2016) Sentinel-1-based flood mapping: a fully automated processing chain. International Journal of Remote Sensing, 37(13), 2990–3004. https://doi.org/10.1080/01431161.2016.1192304.

Vaze J, Mateo CM, Nguyen C, Marvanek S, Ticehurst C, Teng J, Wang B, Austin J, Montazeri M, Kim S, Lerat J, Yang A, Merrin L and Chilcott C (2025) Hydrodynamic model development, implementation and validation for the Richmond River catchment in Northern Rivers NSW Australia. CSIRO, Australia.

Xu H (2006) Modification of normalised difference water index (NDWI) to enhance open water features in remotely sensed imagery. International Journal of Remote Sensing 27, 3025-3033. doi:10.1080/01431160600589179.

Zhou Z-S, Parker A, Brindle L, Rosenqvist A, Caccetta P and Held A (2020) Initial NovaSAR-1 Data Processing and Imagery Evaluation. IGARSS 2020 - IEEE International Geoscience and Remote Sensing Symposium, 2020, pp. 6154–6157.

